Replication-related control over cell division in *Escherichia coli* is growth-rate dependent

Sriram Tiruvadi-Krishnan[1*], Jaana Männik[1*], Prathitha Kar[2,3], Jie Lin[2,4], Ariel Amir[2], Jaan Männik[1]

[1]*Department of Physics and Astronomy, University of Tennessee, Knoxville, TN 37996, USA*

[2]*John A. Paulson School of Engineering and Applied Sciences,* [3]*Department of Chemistry and Chemical Biology, Harvard University, Cambridge, MA 02134, USA*

[4]*Center for Quantitative Biology and Peking-Tsinghua Joint Center for Life Sciences, Academy for Advanced Interdisciplinary Studies, Peking University, Beijing, China*

Corresponding authors: Jaan Männik; JMannik@utk.edu; phone: +1 (865) 974 6018

Ariel Amir; arielamir@seas.harvard.edu; phone: +1 (617) 495-5818

* - Equal contribution

Summary

How replication and division processes are coordinated in the cell cycle is a fundamental yet poorly understood question in cell biology. In *Escherichia coli* different data sets and models have supported a range of conclusions from one extreme where these two processes are tightly linked to another extreme where these processes are completely independent of each other. Using high throughput optical microscopy and cell cycle modeling, we show that in slow growth conditions replication and division processes are strongly correlated, indicating a significant coupling between replication and division. This coupling weakens as the growth rate of cells increases. Our data suggest that the underlying control mechanism in slow growth conditions is related to unreplicated chromosome blocking the onset of constriction at the midcell. We show that the nucleoid occlusion protein SlmA does not play a role in this process and neither do other known factors involved in positioning bacterial Z-ring relative to the chromosome. Altogether this work reconciles different ideas from the past and brings out a more nuanced role of replication in controlling the division process in a growth-rate dependent manner.

Keywords: cell cycle checkpoint, cell division, FtsN, cell cycle modeling, *Escherichia coli*, microfluidics

Introduction

The studies addressing coordination between DNA replication and cell division cycles in *Escherichia coli* date back more than half a century and are still being strongly influenced by the classic Cooper-Helmstetter (CH) model [1]. The latter postulates that cell division completes a period of constant duration, referred to as D-period, after the termination of replication. The model also proposed that the replication period C is growth rate independent in a range of faster growth rates. A constant D-period, which was found to be independent of the growth rate in faster growth rates, would imply that cell division is tightly coupled to replication termination. These predictions have been revisited more recently using single-cell measurements. A good match between the CH model and data was found but only under a further assumption that the C+D period depends on the growth rate in a specific way [2].

As a new element for cell cycle control going beyond the CH model, the adder concept has been introduced [3-7]. In the adder model cells add a constant volume increment during the cell cycle irrespective of their size at birth. In some of these models, the increment is assumed to be added between two consecutive replication events, and cell division is still thought to be tightly coupled to replication [3, 6, 7]. In others, the increment is added from cell birth to division [4, 5, 8]. In these latter models, replication does not play any role in the division process. The latter conclusion has also been drawn by some experimental works which have not relied on cell cycle modeling [9, 10]. As the middle ground of these opposing views, Micali *et al.* have proposed a model postulating that division is controlled concurrently by replication and division-related processes; whichever of these processes completes the latest will trigger cell division [11, 12]. In this concurrent-processes model replication and division related processes are competing with each other in triggering cell division in all growth conditions.

Cell division occurs when two daughter cells separate from each other. This event can be determined from single-cell time-lapse measurements. The existing models predict the timing and cell sizes at this event.

However, it is well-known that the separation of daughter cells results from a long sequence of biochemical processes that only culminate with the separation of two daughter cells [13, 14]. The question arises on what initiates this process sequence and how this initiation is linked to the replication cycle of the chromosome. Previous research has identified that cell division in *E. coli* progresses via two distinct stages [15]. The first of these is the formation of the Z-ring at the cell center. This comprises the assembly of FtsZ protofilaments in the mid-cell region [16]. In *E. coli* the protofilaments are linked to the cell membrane by FtsA and ZipA linkers and likely bundled together with ZapA and several other cross-linking proteins [14, 16]. At multi-forked fast growth conditions, the Z-ring forms at cell birth but in slower growth conditions there is a delay between cell birth and Z-ring formation, which is at least in part controlled by the availability of FtsZ [17, 18]. The Z-ring subsequently recruits about 30 different proteins that are involved in septal cell wall synthesis and partitioning of DNA between daughter compartments [19, 20]. The recruitment of these mostly regulatory proteins proceeds in specific order culminating with the recruitment of FtsN to the divisome complex [14, 16, 19, 21-23]. It is hypothesized that FtsN relieves inhibition or activates core septal peptidoglycan synthesis complex consisting of transpeptidase (FtsW) and transglycosylase (FtsI/PBP IIIA) units [24]. There is a significant delay between the formation of the Z-ring and the onset of constriction [15]. The latter was found to be simultaneous with the recruitment of FtsN to the divisome [22]. It is currently unclear why Z-rings form much earlier than constriction is initiated. Furthermore, the experimental studies related to molecular aspects of cell division have not addressed the question of how the recruitment of divisome components is regulated by the replication cycle of the chromosome.

Here, we study how the initiation of constriction is controlled by the replication cycle. We use quantitative high-throughput fluorescent microscopy and a new functional endogenous FtsN construct. The latter allows us to accurately determine the timing for constriction formation. Our data and cell cycle modeling are consistent with an idea that replication is a rate-limiting factor for constriction in slow growth

conditions. However, the limiting role of replication weakens at faster growth rates. Our results furthermore suggest that the onset of constriction is limited by the unreplicated chromosome at the midcell. This limitation is not related to the nucleoid occlusion factor SlmA, the Ter linkage proteins (ZapA, ZapB, and MatP), and FtsK, a DNA translocase.

Results

Constriction formation follows replication termination in different growth conditions.

To understand the link between replication and division cycles we constructed *E. coli* strains where fluorescent fusion proteins labeled both the replisome and the divisome (for details see Materials and Methods, SI Table S1). We used the N-terminal fusion of mCherry to DnaN (beta clamp) [25] or C-terminal fusion of Ypet to ssb (single-strand binding protein) to label the replisome [26]. For the divisome label, we chose FtsN because it is the latest known component to assemble to the divisome and its recruitment has been reported to coincide with the onset of constriction [14, 16, 19, 21-23]. While in previous fluorescent constructs of FtsN the labeled protein was expressed from extra copy plasmids [19, 27, 28], in our construct it was expressed from the native locus. We grew these strains in steady-state conditions in mother machine devices [29, 30]. The doubling times and lengths of these cells were indistinguishable from the WT ones (strain BW27783) when grown in a glycerol medium (Table S2). Note that all measurements were performed at 28 °C where the growth rate is expected to be about 2 times slower than at 37°C [31]. Using the fluorescently labeled strain we followed the timing of replication termination (Trt), onset of FtsN accumulation at mid-cell (Tn) and onset of constriction (Tc) in time-lapse images (Fig. 1A-B). Here all the times are given relative to cell birth. Additionally, we also determined the timing of replication initiation (Tri) and the C-period ($C = Trt - Tri$). We determined Tri, Trt and Tn from the analysis of fluorescent images and Tc from the phase images (for details see Methods). We found Tc to

be delayed relative to Tn on average by about 12 mins (SI Fig. S1). We assign the delay to less sensitive determination of constriction formation from phase images. We therefore use Tn instead of Tc for the timing of the constriction formation in the Figures in the main text while the data on Tc can be found in SI Figures.

We first investigated the correlation between termination and onset of constriction times in slow growth conditions in the M9 glycerol medium (Fig. 1C). The Tn and Trt times were correlated (with a Pearson correlation coefficient $R = 0.94$) as were also Tc and Trt times ($R = 0.92$; SI Fig. S1). The comparable timings and correlations between Tc and Trt time were also present in a different strain which carried ssb-Ypet label for replisome and no divisome label (Fig. S2) indicating that Ypet fusion to FtsN and mCherry fusion to DnaN did not have significant effects on division and replication processes.

In 7% of cells, we found the onset of constriction as measured by Ypet-FtsN (i.e., Tn) occurred before the termination (Trt) (Fig. 1D). When we determined the onset of constriction from the phase images (Tc), in only 1 out of 420 cells termination occurred earlier than the onset of constriction (SI Fig. S1) but as argued earlier the latter estimate is likely less accurate. For 7% of cells, in which the initiation of constriction preceded the termination, the distribution of times $Tn - Trt$ was approximately exponential with a characteristic time of 7 min (inset of Fig. 1D). The latter time is close to the characteristic time that DnaN remains attached to the replication terminus region after completion of replication (3 mins at 37 °C, potentially translating to about 6 mins in our conditions) [25]. Altogether, the fraction of cells in which the termination of replication occurs after the *actual* onset of constriction is much smaller than 7%, if not zero. Interestingly, the distribution of $Tn - Trt$ was also approximately exponential for positive values with a characteristic time of 15 mins (Fig. 1D, inset). The latter suggests the possibility of a single rate-limiting reaction associated with the process of triggering constriction formation that follows the termination, as we elaborate on later.

We next investigated how the above conclusions applied at different growth rates. We repeated these measurements in eight additional different growth media (SI Table S3); in three of these, the growth rates were slower while in the other five the rates were higher than in the measurement discussed above (SI Table S2). In all of these nine growth conditions, the average delay time $\langle Tn - Trt \rangle$ was positive showing that constriction formation follows on average the termination and possibly in all divisions (Fig. 2A, inset). $\langle Tn - Trt \rangle$ showed variation between 20 min to 40 mins in different growth rates except for the slowest growth rate in acetate medium where $\langle Tn - Trt \rangle \approx 65\ min$. Unlike the almost growth rate-independent behavior of $\langle Tn - Trt \rangle$, the normalized delay times, $\langle (Tn - Trt)/Td \rangle$, showed two distinct growth-rate dependent regimes (Fig. 2A). Below about $Td \approx 130$ mins the normalized times decreased as the doubling time increased but above it, the values plateaued reaching about 12% of the cell cycle. A similar cross-over from one regime to another was also seen in Pearson correlation coefficients, $R(Tn, Trt)$ (Fig. 2B). For $Td > 130$ mins the termination of replication and the onset of constriction were highly correlated ($R(Tn, Trt) > 0.85$) and independent of Td, while for $Td < 130$ mins these correlations decreased approximately linearly with the decreasing Td. A similar cross-over behavior could be also seen in plots when the timing of constriction (Tc) was determined from phase images (SI Fig. S3).

The times of termination and constriction initiation were not only correlated but furthermore followed a timer-like relationship, $Tn = Trt + constant$, at slower growth rates. This was evident in plots of Trt vs Tn where linear regression gave a slope of ≈ 1 for longer doubling times (Fig. 2C). The corresponding intercept of the fits was almost independent of the doubling time (SI Fig. S4A). We also found that the distribution of delay times $Tn - Trt$ in a given growth condition was approximately exponential at slower growth rates, as it was for the growth condition described above (SI Fig. S4B). This was also reflected in the coefficient of variation (CV) of these distributions, which was approximately one at longer doubling times (Fig. 2D). The CV values also showed a cross-over at $Td \approx 130$ mins. In shorter doubling times, the CV values decreased and the mode of the $Tn - Trt$ distributions shifted to positive values (SI Fig. S4B).

Altogether, the exponential distribution of delay times and the timer behavior in a range of slow growth conditions suggest a constant rate process linking onset of constriction to replication. The process may result from a single first-order reaction with some rate-limiting component. Irrespective of the details of this process, for $Td > 130$ mins our data is consistent with the idea that some replication related process controls the initiation of constriction but as the doubling times shorten this process becomes less and less rate-limiting.

Model supports checkpoint for constriction to be close to termination in slow growth conditions

The presented data in slow growth conditions suggest that there is a replication-dependent checkpoint for the onset of constriction. However, it may occur before the termination of replication. To narrow down the possible time range for this checkpoint we constructed an analytical model. The model allows us to calculate the $Tn - Trt$ distributions and various statistics related to the processes as a function of the timing of the checkpoint, Tx (Fig. 3A). In the following discussion, we define the normalized time difference $x = (Trt' - Tx)/\langle C \rangle$, namely the time delay between the true termination event, Trt' (as opposed to the *measured* termination event Trt) and the checkpoint Tx. In the above expression $\langle C \rangle$ is the average C-period in a given growth condition. x ranges from 0 to 1, with $x = 0$ corresponding to a checkpoint at the termination and $x = 1$ to one at the initiation of replication. We furthermore assume that when the replication fork reaches a relative distance x from the replication terminus, initiation of constriction occurs with a constant rate r (i.e., consistent with first-order reaction kinetics). The assumption of a single rate constant is based on the approximately exponential distribution for $Tn - Trt$ (for positive values) (Fig. 1D, SI Fig. S4B) as well as the CV of this distribution being approximately equal to 1 (Fig. 2E) in slow growth conditions. The model also accounts for the difference between the measured value of Trt and the actual one (Trt') due to the finite time DnaN remains DNA bound after replication completes. The attachment time of DnaN has been found to be exponentially distributed [25]. As discussed previously, a mean time of $\langle Ta \rangle = 3$ to $6\ mins$ can be expected in our growth conditions.

Under these assumptions, we find that the CV of the $Tn - Trt$ distribution is given by:

$$\mathrm{CV}\,(Tn - Trt) = \frac{\sqrt{\left(\frac{1}{r}\right)^2 + \sigma_C^2 x^2 + \langle Ta\rangle^2}}{\frac{1}{r} - \langle C\rangle x - \langle Ta\rangle}, \quad (1)$$

(see Model in Methods for the derivation). Here, σ_C is the standard deviation for the distribution of C-periods within the cell population. All the quantities except x in eq. 1 (namely $\langle C\rangle$, σ_C, r, $\langle Ta\rangle$) are determined from experiments (see Model in Methods). We compared the predictions of the above formula to the measured CV values in the four slowest growth conditions. Eq. 1 predicts that $CV(Tn - Trt)$ is close to 1 near x = 0 and rises rapidly with increasing x for all growth conditions considered (Fig. 3B). The experimentally measured CV values are thus consistent with the model only when x is close to zero, that is when the constriction is initiated shortly before or at termination.

The Pearson correlation coefficients between Tn and Trt (Fig. 3C) and the slopes of Tn vs Trt linear fits (Fig. 3D), both of which can be derived analytically within the model, also show an agreement with the experimental data only when x is close to zero. In some growth conditions, however, the best agreement between model and data for the slope of Tn vs Trt occurs for larger values of x. The most outlying point in Fig. 3D corresponds to mannose where the data and the model agree at $x = 0.2$. Nonetheless, most data appear to be consistent with the checkpoint at the termination. Indeed, taking $x = 0$, we could explain satisfactorily the entire distribution of $Tn - Trt$ for all slow growth conditions (Fig. 3E).

To further test the model, we also compared correlations and statistics between experimentally determined replication initiation, Tri and constriction initiation, Tn, timings (SI Fig S5 A-D, Table S4). We found that the model agrees with the experimental values of $\mathrm{CV}(Tn - Tri)$ and $R(Tri, Tn)$ in all slow growth conditions for $x < 0.2$ (SI Fig. S5 E-F). In particular, the model predicts the slope of Tn vs Tri to be exactly one for all values of x, which is indeed observed experimentally (SI Fig. S5C). Altogether, the data and the model can be reconciled for the whole dataset if one assumes that the checkpoint is no more

than $0.2C$ from the termination but most likely at the termination. It is important to emphasize that the agreement between the data and model can only be achieved for slow growth conditions ($Td > 130$ mins). For faster growth rates the model and the data do not agree for any values of x. This disagreement can be expected because the model assumes some replication-related process leading to onset of constriction. As argued above, this assumption is not likely valid at faster growth rates.

Constriction can start before replication termination if the divisome is misplaced

Our goal was then to elucidate the molecular mechanism(s) that could be responsible for triggering constriction formation in a replication-dependent manner. Several molecular systems have been identified in the past that couple division and replication cycles in *E. coli* [32]. These include the nucleoid occlusion factor SlmA [33], the Ter linkage proteins ZapA, ZapB, and MatP [34, 35], and the DNA translocase FtsK [36]. The first two of these systems have been implicated in the positioning of the Z-ring relative to the replication terminus region of the chromosome while FtsK can reposition misplaced chromosomes relative to the division plane at the end of constriction [37]. We next asked if any of these systems are responsible for the correlated timing between the termination of replication and initiation of the constriction. We first considered the effects of SlmA, which is proposed to inhibit the formation of the Z-ring before the Ter region of the chromosome moves to the center of the cell in a replication-dependent manner [32, 38]. Its inhibitory effect is believed to be relieved from the mid-cell in the 2nd half of the replication period because SlmA lacks binding sites at the Ter region. By removing SlmA from the cell one would expect the formation of the Z-ring and the constriction to start earlier. In contrast to this prediction, our data show that the $Tn - Trt$ period increased compared to the WT strain in slow growth conditions ($p = 4 \cdot 10^{-4}$; in single tailed Mann-Whitney test, Fig. 4A & Table S5). At the same time $R(Tn, Trt)$ decreased compared to WT but still remained present at a significant level ($R = 0.7$; Fig. 4B). The observations clearly rule out the idea that SlmA is the main factor responsible for the timing of constriction

formation. Rather, the above findings indicate that SlmA affects the timing of constriction indirectly by modulating the activity of some other factor.

Next, we investigated the role of the Ter linkage proteins ZapA, ZapB, and MatP. Unlike SlmA, which acts as an inhibitor, these proteins have been implicated in promoting the formation of the Z-ring [35]. Together ZapA, ZapB, and MatP form a proteinaceous chain that connects the replication terminus region of the chromosome to the Z-ring. For this connection, all three proteins are needed [34]. Since these proteins promote Z-ring formation, removal of either ZapA, ZapB, or MatP from cells should delay Z-ring formation and possibly also the formation of the constriction. Indeed, removal of either of these three proteins increased $\langle Tn - Trt \rangle$ in a statistically significant manner (SI Table S5) although the magnitude of the effect was small (less than 10% of cell cycle time; < 15 mins). The observed small increase in delay in constriction formation indicates that the Ter linkage proteins, similarly to SlmA, are unlikely to be directly involved in timing the constriction formation.

We also investigated the role of FtsK. FtsK has been implicated in segregating the replication terminus region at the onset of constriction [39, 40]. One could expect the unsegregated terminus region to delay constriction closure. Using a translocation defective mutant FtsK K997A [41] we indeed found $\langle Tn - Trt \rangle$ time to increase but the observed effect was again rather small (11 min; 7% of cell cycle time). Thus, all these mutants showed increased $\langle Tn - Trt \rangle$ periods compared to WT cells and slightly lower correlations in $R(Tn, Trt)$ (Fig. 4B) but these effects were small enough to rule out their direct involvement in triggering the constriction formation. The observed small effects of these deletions arise likely via small changes these proteins have on the structure and composition of the divisome, and on the organization of the chromosome.

Although the Min system is not known to directly couple the replication and division processes, it is one of the main determinants for positioning the Z-ring in *E. coli* [32]. In cells with a defective Min system, a

fraction of divisions occurs close to cell poles while the remaining ones still occur in the vicinity of cell middle. Distinguishing polar divisions from mid-cell ones shows that polar divisions can start significantly earlier than the mid-cell ones (Fig. 4C, D). About half of the polar divisions started before replication had terminated. At the same time, the timing of mid-cell divisions was not affected compared to WT cells (inset of Fig. 4D). The findings related to polar divisions rule out the possibility that termination *triggers* constriction formation as such a trigger would violate causality. On the other hand, these data raise the possibility that replicating nucleoids in mid-cell can block constriction formation. According to the previous discussion, this blockage is not dependent on the nucleoid occlusion factor SlmA.

Discussion

We found that the initiation of the constriction and the termination of the replication in *E. coli* were poorly correlated at fast growth rates but the correlations increased as the growth rate slowed reaching $R = 0.94$ for the slowest growth condition. The cross-over from a correlated to uncorrelated regime occurred approximately at $Td \approx 130$ mins, which corresponds to $Td \approx 65$ mins at 37 °C. A similar cross-over also appeared in $CV(Tn - Trt)$ and in the slope of Trt vs Tn when plotted against Td. Furthermore, the distributions of delay times $Tn - Trt$ become approximately exponential for $Td > 130$ mins suggesting that the replication is rate-limiting for the initiation of constriction.

One of our aims was to further elaborate on the coupling mechanism between replication and division cycles. The measurements with the *minC* deletion strain in slow growth conditions showed that in polar divisions initiation of constriction can precede termination of replication while the mid-cell divisions followed the same timings as in WT cells. This finding ruled out the possibility that termination acts as a trigger for constriction formation. Also, the finding ruled out that there can be a diffusible signal that triggers constriction formation which is released at [42] or before termination. The diffusible signal should reach within seconds all cellular locations including mid cell and pole, and it will not lead to observable

differences in the timing of constriction formation. Note that a protein synthesized in response to transcriptional activation is a diffusible signal. The data thus rule out any possible mechanism where initiation of constriction is triggered in response to transcriptional activation of some gene. Instead of being triggered, the data from polar divisions suggested that a replicating and not fully segregated chromosome in the mid-cell blocks constriction formation; that is, replication related processes license the onset of constriction.

Although the coupling between the replication and division cycles appears to involve some form of nucleoid occlusion, it appears not directly related to the nucleoid occlusion factor SlmA. Clearly, there could be some unknown nucleoid occlusion factor that is not identified yet as argued before [35, 43, 44]. It is also possible that there are no additional proteins involved but the nucleoid occlusion arises directly from chromosome coils or transertion linkages [32], which present a steric hindrance for the formation and maturation of the Z-ring. These possibilities should be examined in further studies.

Altogether, our data indicate that there is a mechanism to license division in a replication-dependent manner (Fig. 5). In slow growth conditions, this licensing is rate-limiting for constriction formation. Our modeling studies suggest that the replication-dependent checkpoint occurs most likely at the termination but not earlier than $0.2C$ from the termination. Once the division is licensed, the constriction formation ensues via reaction kinetics which is suggestive of first-order reaction. At faster growth rates some other competing process appears to become rate-limiting. The origin of the "other" process remains to be also determined. Some authors have proposed the rate-limiting factors for the onset of constriction are precursor molecules for peptidoglycan synthesis [10] such as lipid II while others have concluded that it is the protein FtsZ [8]. Further work is thus needed to clarify the origin of this process.

The regulation proposed in Fig. 5 is similar to the concurrent processes model [11, 12] with some differences. First, the concurrent processes model does not consider the initiation of the constriction as a

cell cycle checkpoint. Instead, it predicts the timing and cell size at the division; that is at the end of all division-related processes. Note that all other current cell cycle models in *E. coli* also predict only the end of the division. Second, in the concurrent processes model replication and growth-related processes are both rate-limiting for division in all growth conditions. Our data suggest that replication is rate-limiting for constriction only in slow growth conditions and the concurrency of the processes is only significant at the vicinity of the cross-over region.

In conclusion, our work has shown that cell division is limited by replication-related processes in slow growth conditions but appears to be almost independent of these processes in fast growth. This behavior might explain why some earlier works have inferred that replication and division cycles are completely uncoupled from each other [8-10] while other authors have come to exactly opposite conclusions [1, 2, 6, 7]. Our data furthermore implies that the limitation related to replication processes stems from some yet to be identified form of nucleoid occlusion. This nucleoid occlusion is lifted in a replication-dependent manner. In parallel to this limitation, cells experience other types of licensing conditions that need to be met. Whether all these limiting processes couple to the divisome via the central hub of FtsZ protofilaments or also via other divisome components remains to be elucidated.

Acknowledgments

The authors thank Ethan Garner, Conrad Woldringh and Arieh Zaritsky for useful discussions, Da Yang and Scott Retterer for help in microfluidic chip making. Authors acknowledge technical assistance and material support from the Center for Environmental Biotechnology at the University of Tennessee. A part of this research was conducted at the Center for Nanophase Materials Sciences, which is sponsored at Oak Ridge National Laboratory by the Scientific User Facilities Division, Office of Basic Energy Sciences, U.S. Department of Energy. This work has been supported by the US-Israel BSF research grant 2017004 (JM),

293 the National Institutes of Health award under R01GM127413 (JM), NSF CAREER 1752024 (AA) and NSF

294 award 1806818 (PK).

295

296 **Conflict of interest**

297 The authors declare that they have no conflicts of interest with the contents of this article.

Figures

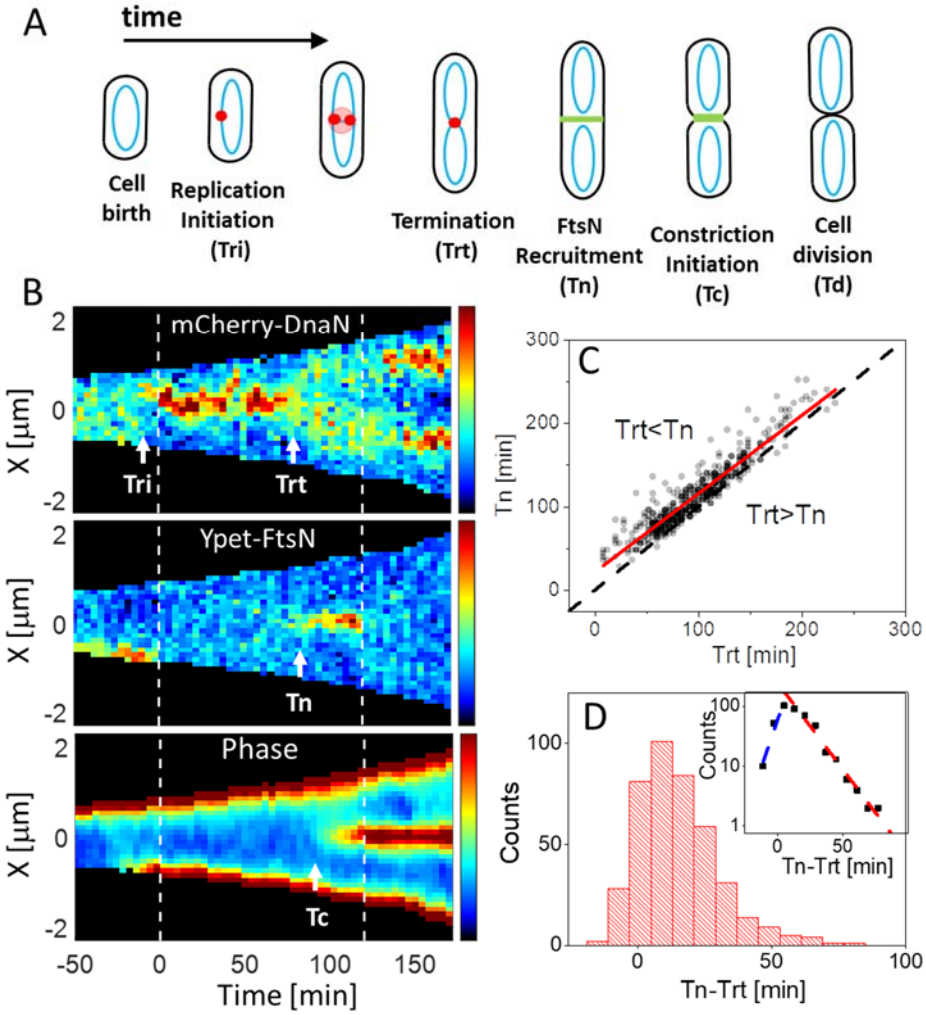

Figure 1. Timing of constriction formation and recruitment of FtsN relative to termination of replication in slow growth conditions. (A) Schematics for the main cell cycle events and timings that are determined from time-lapse measurements. (B) Kymographs of fluorescent and phase signals for a representative cell grown in M9 glycerol medium. Dashed vertical lines indicate cell division events. Red corresponds to high and blue to low-intensity values. Event timings are indicated by arrows. (C) Termination of replication (Trt) vs initiation of constriction (Tn) for a population of cells (N=420). Tn is determined based on the accumulation of Ypet-FtsN signal at mid-cell. The solid red line is a linear fit with ($Tn = 0.94Trt + 22\ \mathrm{mins}$). The dashed black line corresponds to $Trt = Tn$. (D) Distribution of delay times between constriction formation and termination of replication for these cells. Inset shows the same data in a semi-logarithmic plot. The dashed lines are fits to exponential decay. The time constant for the fit at negative times is 7 min and for positive times 15 mins.

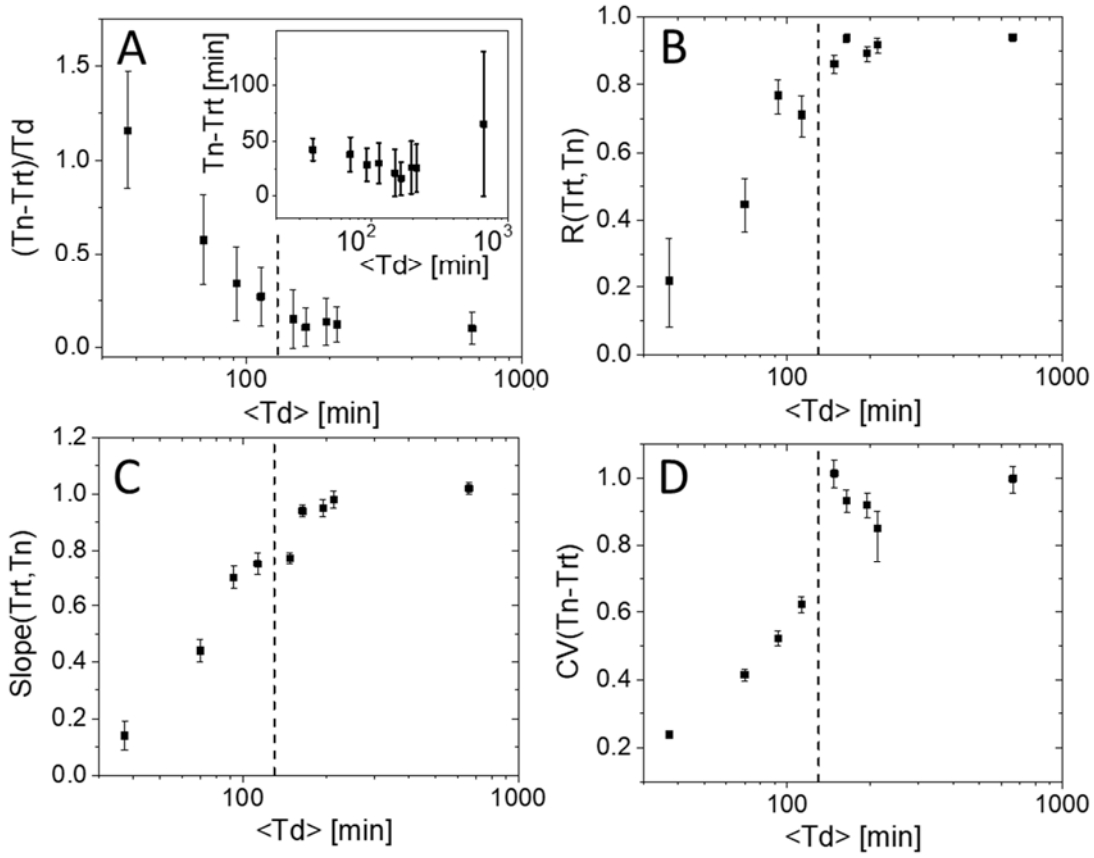

Figure 2. Comparison of timings of constriction initiation and termination of replication in 9 different growth media. From the longest to shortest doubling times the carbon sources used in the media are acetate, alanine, mannose, glycerol, glycerol + trace elements (TrEl), glucose, glycerol+Cas, glucose+Cas, and EZ-Rich defined medium with glucose (for details see Table S3). (A) The average normalized delay time between initiation of constriction and termination of replication as a function of the average doubling time, $\langle Td \rangle$. Inset shows the unnormalized delay time. Error bars in both plots show the std of these quantities within the cell population. (B) Pearson correlation coefficient between Trt and Tn. (C) The slope of Trt vs Tn plot. (D) Coefficient of variation for $Trt - Tn$ distribution. The dashed vertical lines in all plots correspond to $\langle Td \rangle = 130\,\mathrm{min}$. Error bars in (C)-(F) show 95% confidence intervals. For calculation of these intervals see Methods.

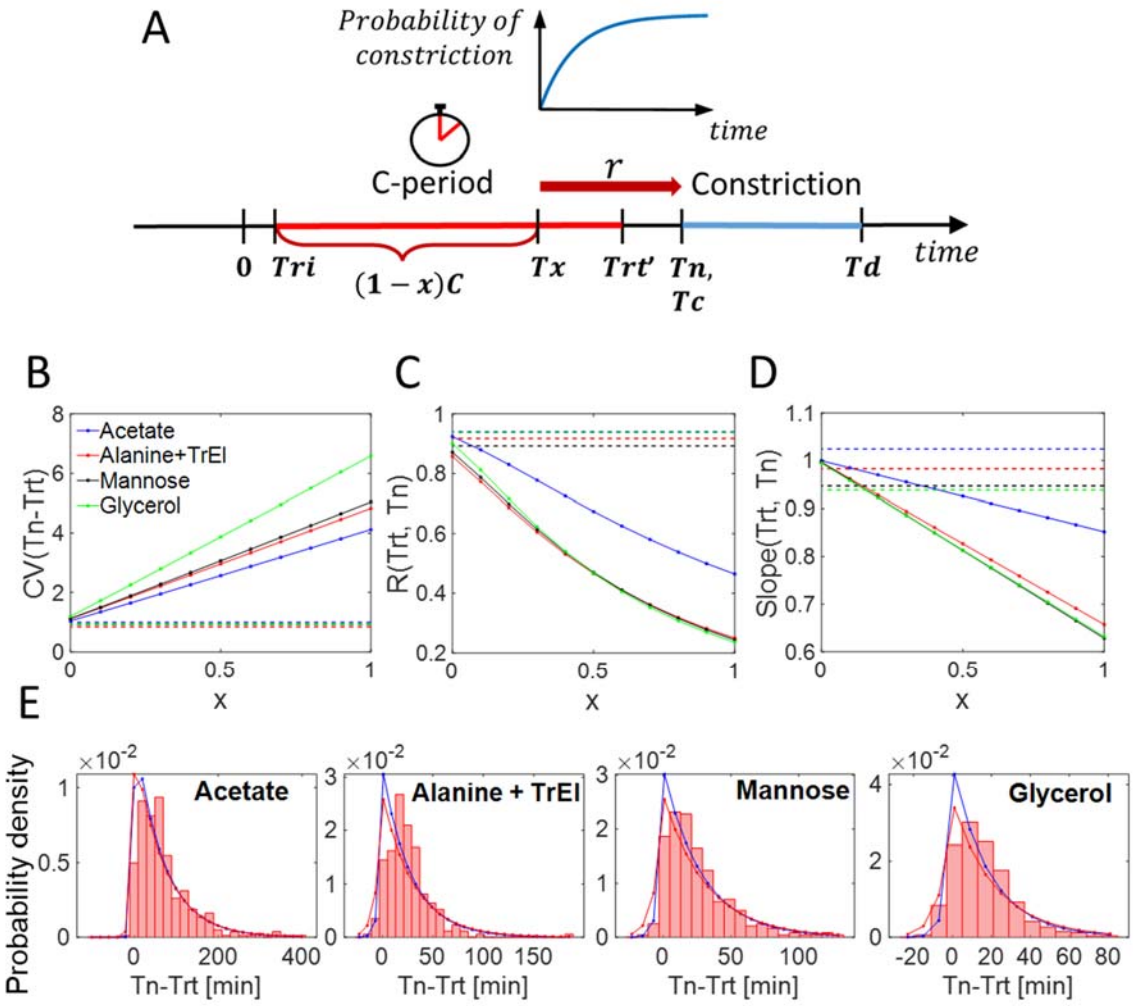

Figure 3: Predictions of model coupling the replication cycle to the onset of constriction. (A) Schematics representing the model. Tx is the timing for the checkpoint that triggers constriction formation. x is the normalized time of this checkpoint from termination. Trt' is the actual time of termination, which differs from the measured time Trt by the detachment time of mCherry-DnaN from the chromosome (see Methods for details). (B) Coefficient of variation of the $Tn - Trt$ distribution, (C) Pearson correlation coefficient between Trt and Tn, and (D) the slope of the linear regression line for Tn vs Trt all plotted as a function of x. In panels (B)-(D) the solid lines show predictions of the model and the dashed horizontal lines the experimental values. Note that only the four slowest growth conditions are considered in these comparisons and $\langle Ta \rangle = 3\ min$. (E) Distribution of $Tn - Trt$ for slow-growth conditions obtained from experiments and from theory for two different values of $\langle Ta \rangle$. The theoretical distributions are given by eq. 20 in Methods and they correspond to $x = 0$. Blue lines correspond to $\langle Ta \rangle = 3\ min$, and red lines to $\langle Ta \rangle = 6\ min$. All other parameters in eq. 20 are determined from the data.

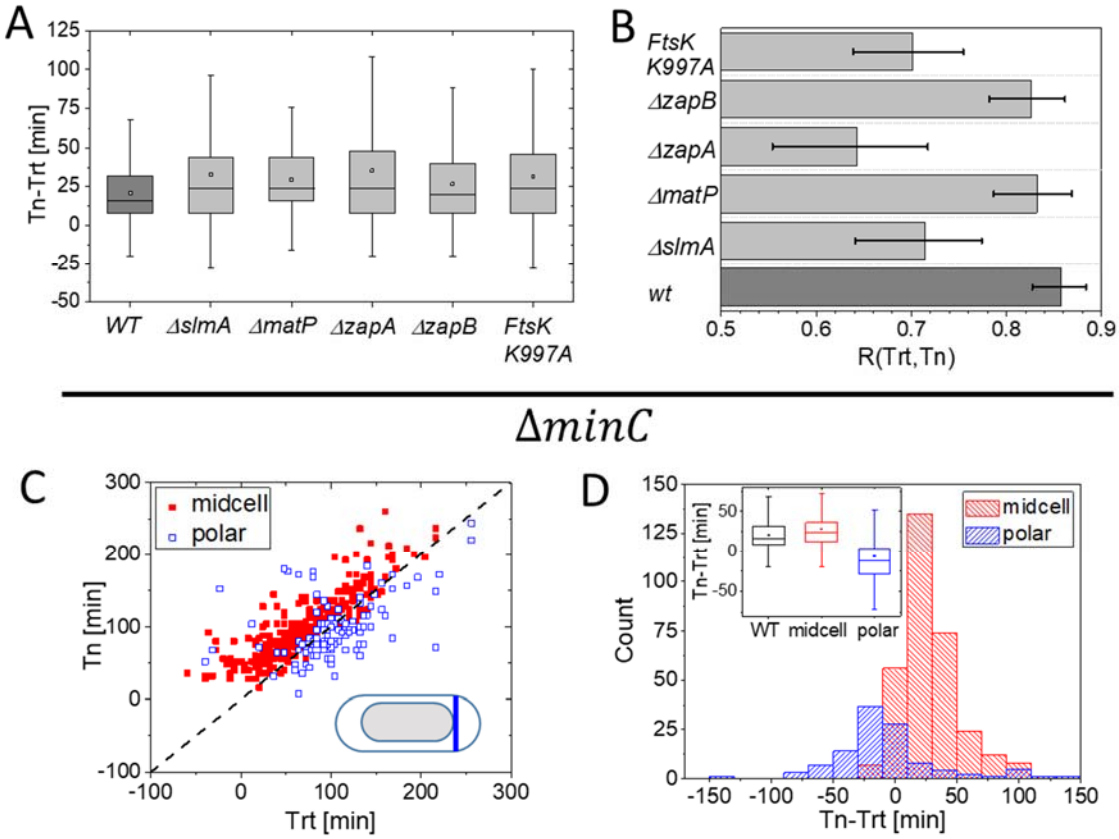

Figure 4. Timings for termination of replication and constriction initiation for different deletion mutants. The deleted gene products have been implicated in coordinating division and replication processes. (A) Delay times between the termination and initiation of constriction for wildtype (WT), $\Delta slmA$, $\Delta matP$, $\Delta zapA$, $\Delta zapB$, and $ftsK\ K997A$ strains. All mutant strains show longer delay times compared to WT strain at $p = 0.05$ level except $\Delta zapA$ (Mann-Whitney test; Table S5). (B) Pearson correlation coefficients between these times for the same strains. Error bars reflect 95% confidence intervals. (C) Termination of replication (Trt) vs initiation of constriction (Tn) for $\Delta minC$ cells. Polar divisions and mid-cell divisions are separately labeled. (D) Distribution of corresponding delay times in this strain. Inset compares the distributions to the corresponding one in WT cells. All measurements were performed in M9 Gly+TrEl medium.

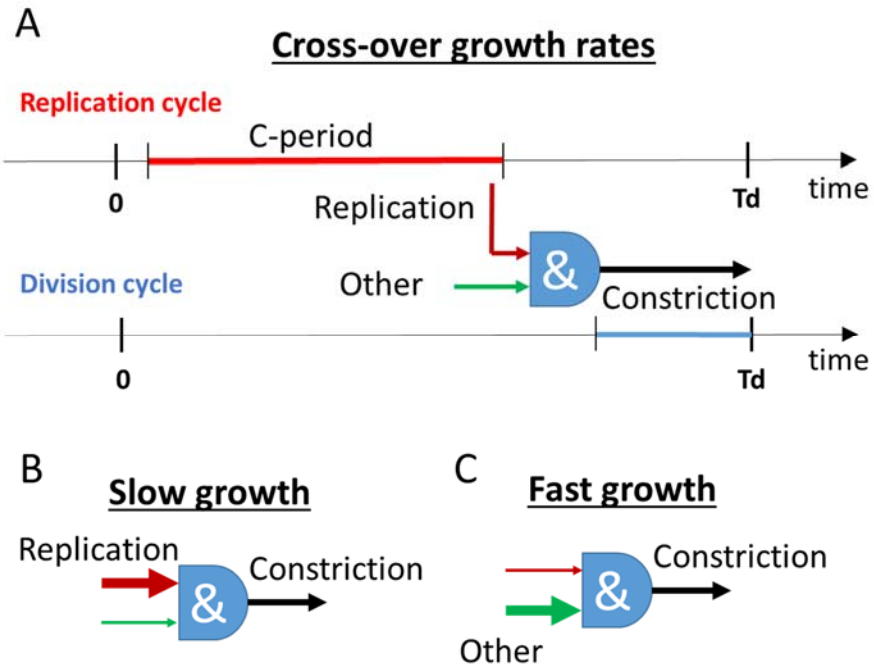

Figure 5. Regulation of constriction formation in different growth rates. (A) Regulation at the cross-over regime where $Td \approx 130\ min$. The corresponding doubling times at 37 °C are expected to be about twice shorter. The replication period is shown by red and the constriction period by blue lines. & sign indicates an integration of different signals. Constriction starts when conditions imposed by the replication and by some "other" yet to be identified processes have been both met. Replication related processes relieve inhibition for initiation of constriction at or shortly before the termination. (B) In slow growth conditions, the onset of constriction is rate-limited by replication-related processes. (C) In fast growth conditions, some unknown "other" process(es) become rate-limiting.

STAR METHODS

KEY RESOURCES TABLE

REAGENT or RESOURCE	SOURCE	IDENTIFIER
Bacterial Strains		
SeeTable S1a		
Chemicals, Peptides, and Recombinant Proteins		
Chloramphenicol	*MilliporeSigma*	Cat#C0378-5G
Kanamycin	*MilliporeSigma*	Cat#K4000-5G
Ampicillin	*MilliporeSigma*	Cat#A0166-5G
Glucose	*MilliporeSigma*	Cat#G8270-100G
Glycerol	*Fisher BioReagents*	Cat#BP229-1
Alanine	*Fisher BioReagents*	Cat#BP369-100
Mannose	*MilliporeSigma*	Cat#M6020-25G
Sodium acetate (acetate)	*MilliporeSigma*	Cat#S5636-250G
Thymine	MP Biomedicals	Cat#0210306025
Casamino acids (Cas)	ACROS Organics	Cat#AC612041000
Isopropanol	Fisher Chemical	Cat#A464-4
Bovine Serum Albumin (BSA)	*MilliporeSigma*	Cat#A7906-10G
M9 minimal media	Teknova.com	Cat#M1902
EZ Rich Defined Medium (EZRDM)	Teknova.com	Cat#M2105
Trace metal elements mixture	Teknova.com	Cat#T1001
Sylgard 184	Dow Corning	N/A
Oligonucleotides		
SeeTable S1b		
Software and Algorithms		
MATLAB R2017a	Mathworks, Inc	RRID:SCR_001622
NIS-Elements	Nikon Instruments Inc.	RRID:SCR_014329
DipImage toolboxes	http://www.diplib.org/	
Python 3.7	https://www.python.org	RRID:SCR_008394
Other		
Nikon Ti-E inverted microscope	Nikon Instruments Inc.	Cat# MEA53100
Nikon Perfect Focus system	Nikon Instruments Inc.	Cat# MEP59390
Andor EMCCD camera	Oxford Instruments	iXon897
O_2 plasma asher	March Instruments	Plasmod
Syringe pump	New Era Pump Systems	Model: NE-1000
Syringe pump	New Era Pump Systems	Model: NE-2000

CONTACT FOR REAGENT AND RESOURCE SHARING

Further information and requests for resources and reagents should be directed to and will be fulfilled by the Lead Contact, Jaan Männik (JMannik@utk.edu).

METHODS

Construction of *E. coli* strains

All *E. coli* strains used in the reported experiments are derivatives of K12 BW27783 obtained from the Yale Coli Genetic Stock Center (CGSC#: 12119). Strains were constructed either by λ-Red engineering [45] and/or by P1 transduction. Where necessary kanamycin resistance gene was removed by expressing the Flp recombinase from plasmid pCP20 [46]. Detailed information of strain genotypes and construction information is listed in Table S1a. Oligonucleotide information is given in Table S1b. For *E. coli* strain engineering, cells were grown in lysogeny broth (LB) and appropriate selective antibiotics.

Growth media and growth conditions

For time-lapse imaging in microfluidic devices, cells were cultured in 9 different growth conditions at 28°C. Detailed information on the media used can be found in SI Table S3.

Cell preparation and culture in microfluidic devices

All bacterial strains were streaked on agar plates containing M9 minimal salts supplemented with 2 mM magnesium sulfate, corresponding carbon sources, and appropriate selective antibiotics. A day before an experiment a less than 10 days old colony was inoculated into 3 ml of EZ Rich Defined Medium (EZRDM, Teknova Inc., CA) or M9 minimal salts media (Teknova Inc., CA) supplemented with corresponding carbon sources, trace metals mixture (Teknova Inc., CA, #T1001), casamino acids (ACROS Organics) and appropriate antibiotics when needed. Unless otherwise indicated, antibiotics were used at 25 µg/ml of kanamycin (Kan) and 25 µg/ml chloramphenicol (CM). For microscopy experiments, cells were grown to an OD_{600} of ~0.1 in a liquid medium and then concentrated ~100x by centrifugation in presence of 0.75 µg/ml of BSA (Bovine Serum Albumin; Millipore Sigma, MO) to minimize clumping of the cells. The resulting solution was used to inoculate microfluidic mother machine devices. The latter were made of PDMS (polydimethylsiloxane) following a previously described procedure [30]. For inoculation 2-3 µl of resuspended concentrated culture was pipetted into the main flow channel of the device. The cells were then let to populate the dead-end channels. Once these channels were sufficiently populated (about 1 hr), tubing was connected to the device, and the flow of fresh M9 medium with corresponding carbon sources and supplements, and BSA (0.75 µg/ml) was started. The flow was maintained by a NE-1000 Syringe Pump (New Era Pump Systems, NY) at 5 µl/min during the entire experiment. To ensure steady-

state growth, the cells were left to grow in channels at least 14 hr (24 hrs for acetate) before imaging started.

Fluorescence microscopy

A Nikon Ti-E inverted fluorescence microscope (Nikon Instruments, Japan) with a 100X NA 1.40 oil immersion phase contrast objective (Nikon Instruments, Japan), was used for imaging the bacteria. Images were captured on an iXon DU897 EMCCD camera (Andor Technology, Ireland) and recorded using NIS-Elements software (Nikon Instruments, Japan). Fluorophores were excited by a 200W Hg lamp through an ND4 and ND8 neutral density filter. Chroma 41004 and 41001 filter cubes (Chroma Technology Corp., VT) were used to record mCherry and Ypet images, respectively. A motorized stage (Prior Scientific Inc., MA) and a Nikon Perfect Focus ® system were utilized throughout time-lapse imaging.

Image analysis

MATLAB, along with the Image Analysis Toolbox and DipImage Toolbox, (http://www.diplib.org/) were used for image analysis. In all analyses of time-lapse recordings, corrections to subpixel shifts between different frames were applied first. These shifts were determined by correlating phase-contrast images in adjacent frames. The cells were then segmented based on phase-contrast images using a custom MATLAB script. The segmented images were used to compile heatmaps of phase and fluorescent images as shown in Fig. 1B. Timings of cell divisions were corrected based on the dissociation of the Ypet-FtsN label from the septum in strains where this label was present. Timings of replication initiation and termination, and initiation of constriction were determined from heatmaps. For the Figures in the main text the replication initiation, Tri, and termination, Trt, timings were determined from the heatmaps of the mCherry-DnaN label (strain STK13). For a detailed procedure see below. In glycerol and glucose+Cas growth media, these timings were also determined using a different strain (JM85), which expressed the ssb-Ypet label. The data from the latter strain are shown in SI Figures. Timings for the onset of FtsN recruitment to the Z-ring, Tn, were determined from Ypet-FtsN heatmaps. The onset of constriction, Tc, was determined from phase hetamaps for both strains.

Determination of Trt timing

In slow growth conditions, there is typically a single termination that increases the number of chromosomes from one to two while at faster growth rates a fraction of cells is born with two chromosomes. To analyze cells born with one and two chromosomes on the same footing we considered

421 the relevant termination for the cells born with two chromosomes to occur in the mother cell. Using this
422 analysis, the termination times of the cell population have a continuous unimodal rather than bimodal
423 distribution. In this distribution, the times of replication termination are negative if these times occur in
424 the mother cell. The two terminations in the mother cell were not exactly synchronous. For a given cell of
425 interest, we determined the timing of the termination for the chromosome that was inherited by this cell.
426
427 **Determination of Tri timing**
428 Similar to the termination, the relevant initiations of replication could occur in the mother cell. In the two
429 fastest growth rates, in EZ-Rich and M9 glucose+CAS the relevant initiations could also occur in the
430 grandmother cells. Our analysis routine did not allow us to determine these events. Also, in these two
431 growth conditions even when the initiations occurred in the mother cell it was rather ambiguous to
432 determine their timing. We, therefore, left out these two growth conditions from the analysis that
433 involved replication initiation (in SI Fig. S5 and Table S4). The timing of replication termination (Trt) could
434 still be reliable determined in these conditions. In other growth media, the initiation occurred either in
435 the mother cell or in the cell of interest. If the initiation occurred in the mother cell then the timing of the
436 initiation of the chromosome that was inherited by the cell of interest was used. The time difference
437 between the two initiations in the mother cell was typically within 8 min interval.
438
439 **Statistical Analysis/Error Analysis**
440 Different distributions of $Tn - Trt$ times were compared using t-test and Mann-Whitney test. For testing
441 Matlab functions *ttest2* and *ranksum* were used, respectively.
442
443 Error bars for the Pearson R-values represent 95% confidence intervals. These intervals were calculated
444 using Fisher's z-transformation [47]. Briefly, based on the measured R-value corresponding z-value was
445 calculated as $z = 1/2\ ln(1 + R/1 - R)$. The 95% confidence intervals for z were calculated as $z_{CI} = [z -$
446 $1.96/\sqrt{N-3}, z + 1.96/\sqrt{N-3}]$ where N is number of measurements for a given R-value. The intervals
447 were then backtransformed for R confidence intervals using $R_{CI} = (exp(2z_{CI}) - 1)/(exp(2z_{CI}) + 1)$.
448
449 Error bars for the coefficient of variation (CV) also represent 95% confidence intervals. These intervals
450 were determined by bootstrapping. Bootstrapping was carried out in Phyton 3.7. by sampling the
451 distributions 10^4 times and verifying that the resulting CV distributions did not change upon further
452 doubling the samples. Percentile intervals were found using *numpy percentile* method.

Model coupling replication and constriction

We assume that cells initiate DNA replication at time Tri and that nucleotides are added to the growing strand of DNA at a constant rate γ. We denote the length of the *E. coli* genome (measured in nucleotide number) as N. Using the central limit theorem, the time taken to reach termination (the C period) is normally distributed with a mean $\frac{N}{\gamma}$ and variance $\frac{N}{\gamma^2}$. The CV of the C period thus scales as $\frac{1}{\sqrt{N}}$ with $N \approx 4 \cdot 10^6$. Thus, the predicted CV is two orders of magnitude smaller than that experimentally observed (SI Table S4), and we conclude that the variability in the C period resulting from stochastic nucleotide addition is negligible. Hence, we can consider the replication process to be happening at a constant velocity v. The time taken for replication to complete is then given by $\frac{N}{v}$, and variability in the C period results from the cell-to-cell variability in v.

Experimentally, the C period and Td are strongly and positively correlated (SI Table S4). This would suggest that the progress of biochemical processes like DNA replication scales with the individual growth rate of the cells. In this case, a slower-growing cell will also replicate at a slower velocity and subsequently have a longer C period. The scaling with growth rate points to a small but non-negligible variability in v within the population of growing cells in a particular media.

Since C is assumed uncorrelated with the initiation time, the time at termination Trt' is thus:

$$Trt' = Tri + C. \quad (1)$$

The evidence for such a "timer" can be found in SI Table S4, which lists the slope of linear regression for Trt vs Tri plots in different growth conditions. As can be seen from SI Table S4, this slope is close to one in slow growth conditions.

In the experiments, the replisome is imaged using a DnaN marker. The DnaN marker is expected to remain attached to the replication terminus region after completion of replication [25]. Thus, in experiments the measured time of termination Trt is,

$$Trt = Trt' + Ta, \quad (2)$$

where Ta is the time for which DnaN stays attached. Ta is assumed to be exponentially distributed with a mean time $\langle Ta \rangle$ = 3-6 mins expected in our growth conditions [25].

We assume Tri to be normally distributed with mean $\langle Tri \rangle$ and standard deviation σ_{ri}, the values for which are determined from experiments. Assuming v to be normally distributed with a mean v_0 and standard deviation σ_v, the C period has an approximately normal distribution with mean $\langle C \rangle = \frac{N}{v_0}$ and variance $\sigma_C^2 = \left(\frac{N\sigma_v}{v_0^2}\right)^2$ when $\sigma_v \ll v_0$. Using Equations 1 and 2, we can determine $\langle C \rangle$ and σ_C^2 to be,

$$\langle C \rangle = \langle Trt - Tri \rangle - \langle Ta \rangle, \tag{3}$$

$$\sigma_C^2 = Var(Trt - Tri) - \langle Ta \rangle^2. \tag{4}$$

$\langle Trt - Tri \rangle$ and $Var(Trt - Tri)$ are the mean and variance of $Trt - Tri$ and are determined directly from experiments (SI Table S4).

In our model, constriction is said to be controlled by an event placed at a locus that is a relative distance of x from the replication terminus. x = 0 denotes the locus is at the terminus while x = 1 denotes a checkpoint at the initiation. Under the assumption that v has a Gaussian distribution with CV$\ll$ 1, we obtain that the checkpoint is triggered after a time ξ from initiation which is normally distributed with mean

$\langle C \rangle (1-x) = \frac{N(1-x)}{v_0}$ and variance $\sigma_C^2 (1-x)^2 = \left(\frac{N(1-x)\sigma_v}{{v_0}^2}\right)^2$. Thus, the checkpoint is said to be reached at time Tx given by,

$$Tx = Tri + \xi\,. \tag{5}$$

Since termination happens at a fraction x along the genome from Tx,

$$Trt' = Tx + \zeta, \tag{6}$$

where ζ is normally distributed with mean $\langle C \rangle x$ and variance $\sigma_C^2\, x^2$. Note that ξ and ζ are correlated with each other with covariance Cov(ξ, ζ) = $\sigma_C^2 x(1-x)$. Both ξ and ζ are also correlated with the C period.

Constriction is assumed to be triggered by the checkpoint at time Tx at a constant rate r. This is based on the fact that the positive values of $Tn - Trt$ are exponentially distributed (Fig. 1D) and the CV of $Tn - Trt$ is close to one (Fig. 2D). Hence, the time at constriction Tn is,

$$Tn = Tx + Txn\,. \tag{7}$$

Txn is exponentially distributed with a mean time = $\frac{1}{r}$. Using eqs. 2 and 6, we get

$$\frac{1}{r} = \langle Tn - Trt \rangle + \langle Ta \rangle + \langle C \rangle x \, . \tag{8}$$

$\langle Tn - Trt \rangle$ can be determined from experiments thus fixing the rate r for different x. x is a free parameter whose value is yet to be determined. Using the experimental results plotted in Fig. 2 and comparing them against the analytical results for varying x, we obtain constraints on the value of x.

We shall first calculate analytically $\mathrm{CV}(Tn - Trt)$ for a given value of x, which can be compared to experimentally determined values shown in Fig. 2D. Using eqs. 2, 6, and 7, we get,

$$Tn - Trt = Txn - (\zeta + Ta). \tag{9}$$

Txn, ζ, Ta are independent of each other. Hence the variance of $Tn - Trt$ is

$$Var(Tn - Trt) = \left(\frac{1}{r}\right)^2 + \sigma_C^2 x^2 + \langle Ta \rangle^2, \tag{10}$$

while the mean is $\frac{1}{r} - (\langle C \rangle x + \langle Ta \rangle)$. Combining the two, we find:

$$\mathrm{CV}\,(Tn - Trt) = \frac{\sqrt{\left(\frac{1}{r}\right)^2 + \sigma_C^2 \cdot x^2 + \langle Ta \rangle^2}}{\frac{1}{r} - \langle C \rangle x - \langle Ta \rangle}. \tag{11}$$

Other statistical constructs presented in Fig. 2 include the Pearson correlation coefficient for Trt, Tn, $R(Tn, Trt)$ and the slope of linear regression for Tn vs Trt plot.

$R(Tn, Trt)$ is defined as,

$$R(Tn, Trt) = \frac{\langle (Tn - \langle Tn \rangle)(Trt - \langle Trt \rangle) \rangle}{\sigma_{rt} \sigma_n}, \tag{12}$$

where σ_{rt} and σ_n are the standard deviations of Trt and Tn, respectively.

From eqs. 5 and 7, we obtain $Tn = Tri + Txn + \xi$. Similarly, from eqs. 1 and 2, $Trt = Tri + C + Ta$. All pairs of variables from Tri, C, Ta, Txn, ξ are uncorrelated with each other except C and ξ which are correlated as remarked earlier. Substituting this into eq. 12, we find the covariance (numerator) to be,

$$\begin{aligned} \langle (Tn - \langle Tn \rangle)(Trt - \langle Trt \rangle) \rangle &= \langle Tri^2 \rangle - \langle Tri \rangle^2 + \langle C\xi \rangle - \langle C \rangle \langle \xi \rangle \\ &= \sigma_{ri}^2 + \sigma_C^2 (1 - x). \end{aligned} \tag{13}$$

σ_n and σ_{rt} are found to be:

$$\sigma_n^2 = \sigma_{ri}^2 + \left(\frac{1}{r}\right)^2 + \sigma_C^2(1-x)^2, \tag{14}$$

$$\sigma_{rt}^2 = \sigma_{ri}^2 + \sigma_C^2 + \langle Ta\rangle^2. \tag{15}$$

Substituting eqs. 13, 14, and 15 into eq. 12, we can obtain $R(Tn, Trt)$. All the parameters in the formula for $R(Tn, Trt)$ can be extracted from experiments while x is a variable.

The slope of the linear regression line for Tn vs Trt is related to $R(Tn, Trt)$ as

$$Slope(Tn, Trt) = \frac{R(Tn, Trt)\sigma_n}{\sigma_{rt}}. \tag{16}$$

This can also be calculated by substituting the values in eq. 13, 14, and 15. This theoretical prediction is compared to the experimental data in Fig. 2C.

Assuming the trigger for the constriction event to be at termination (i.e., $x = 0$), we can obtain the distribution of $Tn - Trt$ times analytically and compare it to experimental distributions. For $x = 0$, we obtain $Tn - Trt = Txn - Ta$. Let us define the random variable $Z = Tn - Trt$. We aim to find its distribution. Using our assumptions that Txn and Ta are independent and exponentially distributed, we obtain the joint probability distribution of Txn and Ta to be,

$$f(t_{xn}, t_a) = \frac{r}{\langle Ta\rangle} e^{-r\, t_{xn}} \cdot e^{-\frac{t_a}{\langle Ta\rangle}}. \tag{17}$$

For $z \geq 0$,

$$P_+(Z \leq z) = \frac{r}{\langle Ta\rangle}\int_0^\infty e^{-\frac{t_a}{\langle Ta\rangle}}\, dt_a \int_0^{t_a+z} e^{-rt_{xn}}\, dt_{xn} = 1 - \frac{e^{-rz}}{1 + r\langle Ta\rangle}, \tag{18}$$

with $P_+(Z \leq z)$ the cumulative distribution function (CDF) of Z for $z \geq 0$. Similarly, for $z \leq 0$, we obtain,

$$P_-(Z \leq z) = \frac{r}{\langle Ta\rangle}\int_{-z}^\infty e^{-\frac{t_a}{\langle Ta\rangle}}\, dt_a \int_0^{t_a+z} e^{-rt_{xn}}\, dt_{xn} = \frac{r\langle Ta\rangle}{1 + r\langle Ta\rangle} e^{\frac{z}{\langle Ta\rangle}}. \tag{19}$$

Therefore, we find that the probability distribution of $Z = Tn - Tri$, $g(z) = \frac{dP(z)}{dz}$ is

$$g(z) = \frac{1}{\frac{1}{r} + \langle Ta\rangle}\begin{cases} e^{-rz}, & z \geq 0 \\ e^{\frac{z}{\langle Ta\rangle}}, & z < 0 \end{cases}. \tag{20}$$

The parameters can be determined using the experimental data as discussed before.

Finally, we also investigate the relationship between replication initiation timing Tri and timing for initiation of constriction Tn. As before we will calculate the relevant statistics as a function of x. We will rely on the fact that $Tn = Tri + Txn + \xi$, and that Tri, Txn and ξ are uncorrelated. The variance of $Tn - Tri$ is found to be,

$$Var(Tn - Tri) = \left(\frac{1}{r}\right)^2 + \sigma_C^2\,(1-x)^2, \tag{21}$$

while the mean of $Tn - Tri = \frac{1}{r} + \langle C\rangle(1-x)$. Thus, $\mathrm{CV}(Tn - Tri)$ is found to be,

$$\mathrm{CV}(Tn - Tri) = \frac{\sqrt{\left(\frac{1}{r}\right)^2 + \sigma_C^2(1-x)^2}}{\frac{1}{r} + \langle C\rangle(1-x)}. \tag{22}$$

Other statistical constructs which we calculate include the Pearson correlation coefficient for Tri, Tn, $R(Tn, Tri)$ and the slope of linear regression for Tn vs Tri plot.

$R(Tn, Tri)$ is defined as,

$$R(Tn, Tri) = \frac{\langle (Tn - \langle Tn\rangle)(Tri - \langle Tri\rangle)\rangle}{\sigma_{ri}\sigma_n}, \tag{23}$$

Using $Tn = Tri + Txn + \xi$, we find the numerator to be:

$$\langle (Tn - \langle Tn\rangle)(Tri - \langle Tri\rangle)\rangle = \sigma_{ri}^2. \tag{24}$$

The quantity σ_{ri} is directly inferred from experiments while σ_n is calculated using eq. 14. Substituting the values into eq. 23, we can obtain $R(Tn, Tri)$. The slope of the linear regression line between Tn and Tri is related to $R(Tn, Tri)$ as

$$Slope(Tn, Tri) = \frac{R(Tn, Tri)\sigma_n}{\sigma_{ri}} = 1. \tag{25}$$

Hence, the slope of the linear regression line for Tn vs Tri is always one independent of growth conditions. In other words, within the model Tn is related to Tri via a timer. In the four slowest growing conditions, the slope between Tn vs Tri is indeed close to 1 as shown in SI Fig. S5C.

References

1. Cooper, S., and Helmstetter, C.E. (1968). Chromosome replication and division cycle of *Escherichia coli* B/r. Journal of Molecular Biology *31*, 519-540.
2. Wallden, M., Fange, D., Lundius, E.G., Baltekin, O., and Elf, J. (2016). The synchronization of replication and division cycles in individual *E. coli* cells. Cell *166*, 729-739.
3. Amir, A. (2014). Cell size regulation in bacteria. Phys. Rev. Lett. *112*, 208102.
4. Campos, M., Surovtsev, I.V., Kato, S., Paintdakhi, A., Beltran, B., Ebmeier, S.E., and Jacobs-Wagner, C. (2014). A constant size extension drives bacterial cell size homeostasis. Cell *159*, 1433-1446.
5. Taheri-Araghi, S., Bradde, S., Sauls, J.T., Hill, N.S., Levin, P.A., Paulsson, J., Vergassola, M., and Jun, S. (2015). Cell-size control and homeostasis in bacteria. Curr. Biol. *25*, 385-391.
6. Ho, P.-Y., and Amir, A. (2015). Simultaneous regulation of cell size and chromosome replication in bacteria. Frontiers in Microbiology *6*, 662.
7. Witz, G., van Nimwegen, E., and Julou, T. (2019). Initiation of chromosome replication controls both division and replication cycles in *E. coli* through a double-adder mechanism. Elife *8*, 48063.
8. Si, F.W., Le Treut, G., Sauls, J.T., Vadia, S., Levin, P.A., and Jun, S. (2019). Mechanistic origin of cell-size control and homeostasis in bacteria. Curr. Biol. *29*, 1-11.
9. Bernander, R., and Nordstrom, K. (1990). Chromosome replication does not trigger cell division in *Escherichia coli*. Cell *60*, 365-374.
10. Harris, L.K., and Theriot, J.A. (2016). Relative Rates of Surface and Volume Synthesis Set Bacterial Cell Size. Cell *165*, 1479-1492.
11. Micali, G., Grilli, J., Marchi, J., Osella, M., and Lagomarsino, M.C. (2018). Dissecting the control mechanisms for DNA replication and cell division in *E. coli*. Cell Reports *25*, 761-771.
12. Micali, G., Grilli, J., Osella, M., and Lagomarsino, M.C. (2018). Concurrent processes set *E. coli* cell division. Science Advances *4*, aau3324.
13. Willis, L., and Huang, K.C. (2017). Sizing up the bacterial cell cycle. Nat. Rev. Microbiol. *15*, 606-620.
14. Haeusser, D.P., and Margolin, W. (2016). Splitsville: structural and functional insights into the dynamic bacterial Z ring. Nat. Rev. Microbiol. *14*, 305-319.
15. Aarsman, M.E.G., Piette, A., Fraipont, C., Vinkenvleugel, T.M.F., Nguyen-Disteche, M., and den Blaauwen, T. (2005). Maturation of the *Escherichia coli* divisome occurs in two steps. Mol. Microbiol. *55*, 1631-1645.
16. Du, S.S., and Lutkenhaus, J. (2019). At the heart of bacterial cytokinesis: the Z ring. Trends in Microbiology *27*, 781-791.
17. Männik, J., Walker, B.E., and Männik, J. (2018). Cell cycle-dependent regulation of FtsZ in *Escherichia coli* in slow growth conditions. Mol. Microbiol. *110*, 1030-1044.
18. Walker, B.E., Mannik, J., and Mannik, J. (2020). Transient membrane-linked FtsZ assemblies precede Z-ring formation in *Escherichia coli*. Curr. Biol. *30*, 499-508.
19. Liu, B., Persons, L., Lee, L., and de Boer, P.A.J. (2015). Roles for both FtsA and the FtsBLQ subcomplex in FtsN-stimulated cell constriction in *Escherichia coli*. Mol. Microbiol. *95*, 945-970.

20. Egan, A.J.F., Errington, J., and Vollmer, W. (2020). Regulation of peptidoglycan synthesis and remodelling. Nat. Rev. Microbiol. *18*, 446-460.

21. Weiss, D.S. (2015). Last but not least: new insights into how FtsN triggers constriction during *Escherichia coli* cell division. Mol. Microbiol. *95*, 903-909.

22. Daley, D.O., Skoglund, U., and Soderstrom, B. (2016). FtsZ does not initiate membrane constriction at the onset of division. Scientific Reports *6*, srep33138.

23. Boes, A., Olatunji, S., Breukink, E., and Terrak, M. (2019). Regulation of the peptidoglycan polymerase activity of PBP1b by antagonist actions of the core divisome proteins FtsBLQ and FtsN. MBio *10*, 01912-01918.

24. Taguchi, A., Welsh, M.A., Marmont, L.S., Lee, W., Sjodt, M., Kruse, A.C., Kahne, D., Bernhardt, T.G., and Walker, S. (2019). FtsW is a peptidoglycan polymerase that is functional only in complex with its cognate penicillin-binding protein. Nature Microbiology *4*, 587-594.

25. Moolman, M.C., Krishnan, S.T., Kerssemakers, J.W.J., van den Berg, A., Tulinski, P., Depken, M., Reyes-Lamothe, R., Sherratt, D.J., and Dekker, N.H. (2014). Slow unloading leads to DNA-bound beta(2)-sliding clamp accumulation in live *Escherichia coli* cells. Nature Communications *5*, 11.

26. Reyes-Lamothe, R., Sherratt, D.J., and Leake, M.C. (2010). Stoichiometry and architecture of active DNA replication machinery in *Escherichia coli*. Science *328*, 498-501.

27. Soderstrom, B., Chan, H., Shilling, P.J., Skoglund, U., and Daley, D.O. (2018). Spatial separation of FtsZ and FtsN during cell division. Mol. Microbiol. *107*, 387-401.

28. Busiek, K.K., and Margolin, W. (2014). A role for FtsA in SPOR-independent localization of the essential Escherichia coli cell division protein FtsN. Mol. Microbiol. *92*, 1212-1226.

29. Wang, P., Robert, L., Pelletier, J., Dang, W.L., Taddei, F., Wright, A., and Jun, S. (2010). Robust growth of *Escherichia coli*. Curr. Biol. *20*, 1099-1103.

30. Yang, D., Jennings, A.D., Borrego, E., Retterer, S.T., and Männik, J. (2018). Analysis of factors limiting bacterial growth in PDMS mother machine devices. Frontiers in Microbiology *9*, 871.

31. Herendeen, S.L., Vanbogelen, R.A., and Neidhardt, F.C. (1979). Levels of major proteins of Escherichia coli during growth at different temperatures. J. Bacteriol. *139*, 185-194.

32. Männik, J., and Bailey, M.W. (2015). Spatial coordination between chromosomes and cell division proteins in *Escherichia coli*. Frontiers in Microbiology *6*, 306.

33. Bernhardt, T.G., and de Boer, P.A.J. (2005). SlmA, a nucleoid-associated, FtsZ binding protein required for blocking septal ring assembly over chromosomes in *E. coli*. Mol. Cell *18*, 555-564.

34. Espeli, O., Borne, R., Dupaigne, P., Thiel, A., Gigant, E., Mercier, R., and Boccard, F. (2012). A MatP-divisome interaction coordinates chromosome segregation with cell division in *E. coli*. EMBO J. *31*, 3198-3211.

35. Bailey, M.W., Bissichia, P., Warren, B.T., Sherratt, D.J., and Männik, J. (2014). Evidence for divisome localization mechanisms independent of the Min system and SlmA in *Escherichia coli*. PLoS Genet. *10*, 1004504.

36. Sherratt, D.J., Arciszewska, L.K., Crozat, E., Graham, J.E., and Grainge, I. (2010). The *Escherichia coli* DNA translocase FtsK. Biochemical Society Transactions *38*, 395-398.

37. Männik, J., Bailey, M.W., O'Neill, J.C., and Männik, J. (2017). Kinetics of large-scale chromosomal movement during asymmetric cell division in Escherichia coli. PLoS Genet. *13*, e1006638.

38. Cho, H.B., McManus, H.R., Dove, S.L., and Bernhardt, T.G. (2011). Nucleoid occlusion factor SlmA is a DNA-activated FtsZ polymerization antagonist. Proc. Natl. Acad. Sci. U. S. A. *108*, 3773-3778.

39. Stouf, M., Meile, J.-C., and Cornet, F. (2013). FtsK actively segregates sister chromosomes in *Escherichia coli*. Proc. Natl. Acad. Sci. U. S. A. *110*, 11157-11162.

40. Galli, E., Midonet, C., Paly, E., and Barre, F.X. (2017). Fast growth conditions uncouple the final stages of chromosome segregation and cell division in Escherichia coli. PLoS Genet. *13*, 1006702.

41. Barre, F.X., Aroyo, M., Colloms, S.D., Helfrich, A., Cornet, F., and Sherratt, D.J. (2000). FtsK functions in the processing of a Holliday junction intermediate during bacterial chromosome segregation. Genes Dev. *14*, 2976-2988.

42. Mulder, E., and Woldringh, C.L. (1989). Actively replicating nucleoids influence positioning of division sites in *Escherichia coli* filaments forming cells lacking DNA. J. Bacteriol. *171*, 4303-4314.

43. Cambridge, J., Blinkova, A., Magnan, D., Bates, D., and Walker, J.R. (2014). A replication-inhibited unsegregated nucleoid at mid-cell blocks Z-ring formation and cell division independently of SOS and the SlmA nucleoid occlusion protein in *Escherichia coli*. J. Bacteriol. *196*, 36-49.

44. Rodrigues, C.D.A., and Harry, E.J. (2012). The Min system and nucleoid occlusion are not required for identifying the division site in *Bacillus subtilis* but ensure its efficient utilization. PLoS Genet. *8*, 1002561.

45. Datsenko, K.A., and Wanner, B.L. (2000). One-step inactivation of chromosomal genes in *Escherichia coli* K-12 using PCR products. Proc. Natl. Acad. Sci. U. S. A. *97*, 6640-6645.

46. Cherepanov, P.P., and Wackernagel, W. (1995). Gene disruption in *Escherichia coli* - TcR and Km(R) cassettes with the option of flp-catalyzed excision of the antibiotic-resistance determinant. Gene *158*, 9-14.

47. Nicholls, A. (2014). Confidence limits, error bars and method comparison in molecular modeling. Part 1: The calculation of confidence intervals. Journal of Computer-Aided Molecular Design *28*, 887-918.